Self-assembled bifunctional surface mimics an enzymatic and templating protein for the synthesis of a metal oxide semiconductor

David Kisailus*†, Quyen Truong†, Yosuke Amemiya*†‡, James C. Weaver*†, and Daniel E. Morse*†§¶

*Institute for Collaborative Biotechnologies, †Materials Research Laboratory and California NanoSystems Institute, and §Department of Molecular, Cellular, and Developmental Biology, University of California, Santa Barbara, CA 93106-9610

Edited by John A. Carbon, University of California, Santa Barbara, CA, and approved February 14, 2006 (received for review September 28, 2005)

The recent discovery and characterization of silicatein, a mineral-synthesizing enzyme that assembles to form the filamentous organic core of the glassy skeletal elements (spicules) of a marine sponge, has led to the development of new low-temperature synthetic routes to metastable semiconducting metal oxides. These protein filaments were shown *in vitro* to catalyze the hydrolysis and structurally direct the polycondensation of metal oxides at neutral pH and low temperature. Based on the confirmation of the catalytic mechanism and the essential participation of specific serine and histidine residues (presenting a nucleophilic hydroxyl and a nucleophilicity-enhancing hydrogen-bonding imidazole nitrogen) in silicatein's catalytic active site, we therefore sought to develop a synthetic mimic that provides both catalysis and the surface determinants necessary to template and structurally direct heterogeneous nucleation through condensation. Using lithographically patterned poly(dimethylsiloxane) stamps, bifunctional self-assembled monolayer surfaces containing the essential catalytic and templating elements were fabricated by using alkane thiols microcontact-printed on gold substrates. The interface between chemically distinct self-assembled monolayer domains provided the necessary juxtaposition of nucleophilic (hydroxyl) and hydrogen-bonding (imidazole) agents to catalyze the hydrolysis of a gallium oxide precursor and template the condensed product to form gallium oxohydroxide (GaOOH) and the defect spinel, gamma-gallium oxide (γ-Ga_2O_3). Using this approach, the production of patterned substrates for catalytic synthesis and templating of semiconductors for device applications can be envisioned.

biomimetic | enzyme | hydrolysis | self-assembly

Lessons learned from nature have recently been embraced by materials scientists to harness the mild yet efficient chemical routes used in biological systems for the development of nanofabricated engineering systems (1). Enzymes are highly evolved bimolecular catalysts used to facilitate reactions that might otherwise be kinetically prohibited. Through the well defined orchestration of interactions between chemical moieties in unique conformations dictated by the genetic code and protein self-assembly, incoming substrates are oriented preferentially to stabilize transition states that channel specific reaction pathways. Serine-based hydrolases are one such class of enzymes that facilitate the hydrolysis of a wide range of compounds. Through a unique combination of nucleophilic and hydrogen-bonding agents, a weak transitory bond is formed between the two moieties in the catalytic center (Fig. 1*A*) that enhances the nucleophilicity of the hydroxyl oxygen, facilitating nucleophilic attack on substrate molecules leading to hydrolysis (2).

We have discovered one such hydrolase that, rather than existing as a monomeric functional unit, assembles to form the filamentous organic core of the glassy skeletal elements (spicules) of the marine sponge, *Tethya aurantia* (3–5). Spicule biosynthesis in *T. aurantia* apparently is mediated by these protein filaments that serve as both catalysts and templates for the deposition of silica (3, 4, 6–9). These filaments consist primarily of three highly similar subunits called silicateins (for *silica* pro*teins*). Molecular cloning and sequence analyses revealed the surprising fact that these proteins are members of a well known superfamily of proteolytic and hydrolytic enzymes (3). Based on this discovery, the intact filaments, and their constituent monomers obtained from disaggregation of the filaments or those produced from recombinant DNA templates cloned in bacteria, were subsequently shown *in vitro* to catalyze the hydrolysis and structurally direct the polycondensation of silicon alkoxide precursors to form silica and poly(silsesquioxanes) at

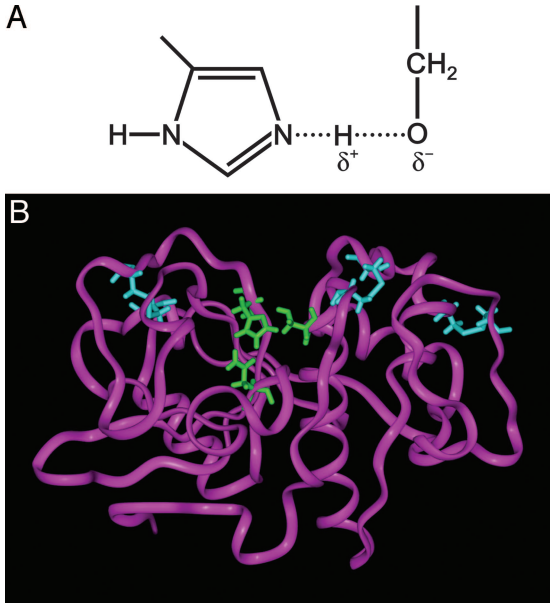

Fig. 1. Catalytic site of serine-containing hydrolase enzymes, including silicatein. (*A*) Schematic of the essential chemical moieties in a serine-hydrolase active site. The proximity of the nitrogen from the imidazole ring to the hydroxyl of serine facilitates hydrogen-bonding; this enhances the nucleophilicity of the oxygen, thus potentiating catalytic hydrolysis reactions. Weakening of the O–H bond is indicated by the dashed line. (*B*) Ribbon model of silicatein α from an energy minimization program (INSIGHT II). The ribbon model depicted here highlights (in green) the catalytic site in which the nucleophilic serine is presented to a hydrogen-bonding imidazole that enhances the hydrolytic activity of the enzyme (6).

Conflict of interest statement: No conflicts declared.

This paper was submitted directly (Track II) to the PNAS office.

Abbreviations: GaOOH, gallium oxohydroxide; γ-Ga_2O_3, gamma-gallium oxide; HB, hydrogen-bonding; NP, nucleophilic; SAM, self-assembled monolayer; TEM, transmission electron microscopy.

‡Present address: Department of Biotechnology, Tokyo University of Agriculture and Technology, 2-24-16 Naka-cho Koganei, Tokyo 184-8588, Japan.

¶To whom correspondence should be sent at the * address. E-mail: d_morse@lifesci.ucsb.edu.

www.pnas.org/cgi/doi/10.1073/pnas.0508488103

Table 1. Contact-angle measurements of ω-terminated SAMs

SAM ω-functionality	Advancing angle, °	Standard deviation, °	Receding angle, °	Standard deviation, °
Methyl	98	5	90	5
Hydroxyl	16	3	9	3
Carboxylic acid	30	3	19	2
Imidazole	44	2	27	4
Gold (no SAM)	66	3	45	2

neutral pH and low temperature (4). Extension of this catalytic mechanism for the controlled room-temperature synthesis of metal oxide semiconductors such as titanium dioxide (9) and gallium oxide (10) from alkoxide-like molecular precursors was also successful. Genetic engineering by site-directed mutagenesis confirmed the mechanism of catalysis and the essential participation of specific serine and histidine residues (presenting a nucleophilic hydroxyl and a nucleophilicity-enhancing hydrogen-bonding imidazole nitrogen) in the catalytically active site of the silicateins (Fig. 1*B*) (6). Predictive synthesis of biomimetic diblock copolypeptides (11) based on these results yielded catalytically active molecules that exhibited both silica-synthesizing and structure-directing capabilities. A family of small bifunctional molecules displaying the nucleophilic and hydrogen-bonding amine functionalities characteristic of the enzyme's active site also was shown to be catalytically active (12). Naik *et al.* (13) also used peptides based on those found by Kröger and Sumper (14–16) in the silica made by diatoms to induce and direct the precipitation of silica at low temperatures, although the mechanism was different from that of the silicateins and its biomimetics, because the starting material was silicic acid, and no catalysis of hydrolysis was required.

Recently, we successfully demonstrated the use of a synthetic system that mimics the hydrolytic activity of the silicatein α monomer; this system included a combination of nucleophilic hydroxyl and hydrogen-bonding amine terminated alkane thiols tethered to single crystal gold nanoparticles incubated together in a silicon alkoxide solution (17), leading to the hydrolysis of the precursor and condensation of silica. Although the functionalized gold nanoparticles displayed the unique side chains that afforded hydrolytic activity, they could not provide the periodic arrangement of condensation sites lending to the nanostructured products observed in reactions performed with the native silicatein filaments (10).

Purified enzymes are immobilized on solid surfaces for a diversity of applications ranging from pharmaceutical syntheses, food and fabric preparation, biological and chemical sensors, and fuel cells (18–21). However, the expense and instability of the biomolecular catalysts presently limit the large-scale applicability of this approach. Based on the successful development of the gold nanoparticle-supported bifunctional catalytic mimics of the silicateins, we therefore sought to develop a synthetic mimic that would include a surface upon which both catalysis and heterogeneous nucleation through condensation will occur. Using this approach, the production of patterned substrates for catalytic synthesis and templating of semiconductors for device applications can be envisioned.

Results

Self-Assembled Monolayer (SAM) Characterization. Contact-angle measurements (Table 1) of monofunctionalized surfaces confirmed (22, 23) the absorption and ordering of alkane thiols on the gold surface. Low solid–liquid contact angles were measured for hydrophilic-terminated SAMs (e.g., hydroxyl and carboxylic acid) whereas higher contact angles were observed for more hydrophobic surfaces (e.g., imidazole and methyl) confirming the presentation of the desired ω-functionalities at the solid–liquid interface. Angle-resolved x-ray photoelectron spectroscopy (data not shown) validated these observations. An optical micrograph (Fig. 2) of a bifunctional (hydroxyl-imidazole) surface exposed to water vapor highlighted the line pattern generated from microcontact printing SAMs.

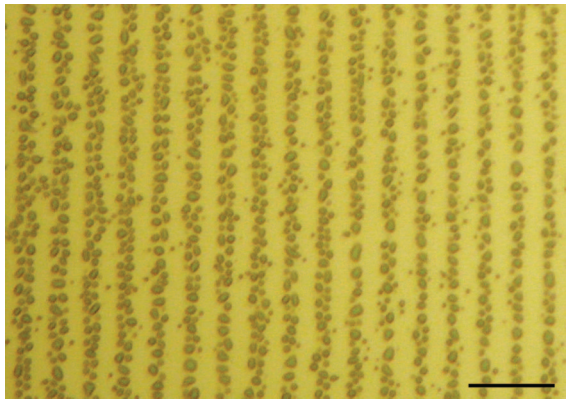

Fig. 2. Optical micrograph of the bifunctional SAM surface exposed to water vapor. Water droplets are observed condensing on the hydrophilic surface whereas none are observed on the hydrophobic surface. (Scale bar: 50 μm.)

Surface Characterization of SAM-Mediated Reaction Products. Wafers expressing bifunctional surfaces that were immersed in aqueous solutions of gallium nitrate were examined by scanning electron microscopy. Fig. 3*A* depicts products formed from the successful hydrolysis and condensation reactions of the gallium nitrate precursor catalyzed by the bifunctional wafer containing the nucleophilic (hydroxyl) and hydrogen-bonding (imidazole) agents (NP-HB surface). Energy-dispersive spectroscopy mapping (Fig. 3*B*) of condensate on the NP-HB biomimetic catalyst revealed a product, localized on the hydroxyl lines, rich in gallium and oxygen. Higher magnification imaging revealed a dense network of layered particles (Fig. 3*C*) condensed upon the hydroxyl-printed lines. Substitution of either essential surface functionality (nucleophile or hydrogen-bonding amine) with a nonactive methyl group rendered the surface hydrolytically inactive (Fig. 3*D*). The NP-HB surface showed a 10-fold-greater particle number density on the hydroxyl lines ($\approx$14.53 $\pm$ 0.62 per μm^2) than on the imidazole lines ($\approx$1.34 $\pm$ 26 per μm^2), with particles on the hydroxyl lines (Fig. 3*E*) less than half the size of particles on the imidazole lines.

To confirm the position of the catalytic interface, samples were removed at short time intervals to establish the location of condensed metal oxide particles. Fig. 3*F* clearly demonstrates significantly more condensed product at the SAM interface after a short reaction period with a substantial decrease in particle number density away from the interface.

Phase Analysis of SAM-Mediated Reaction Products. X-ray diffraction (not shown) demonstrated that the product synthesized at room temperature by the NP-HB bifunctional wafer consisted of both gallium oxohydroxide (GaOOH) [Joint Committee for Powder Diffraction Studies (JCPDS) no. 06-0180] and gamma-gallium oxide (γ-Ga_2O_3) (JCPDS no. 20-0426). Particles deposited on the hydroxyl-terminated lines had diameters approximately half ($\approx$50 nm $\times$ 150 nm; Fig. 4*A*) of those adhering to the imidazole surface (125 nm $\times$ 250 nm; Fig. 4*B*) as measured by transmission electron microscopy (TEM). Representative selected-area electron diffraction patterns of both types of particles confirmed the XRD observations. These results indicate that the smaller particles consisted of γ-Ga_2O_3 (Fig. 4*C*) whereas the larger particles were identified as GaOOH (data not shown). High-resolution TEM (Fig. 4*D*) revealed that the particles formed on the SAMs consisted of highly oriented crystalline aggregates of smaller ($\approx$3 nm) particles. These

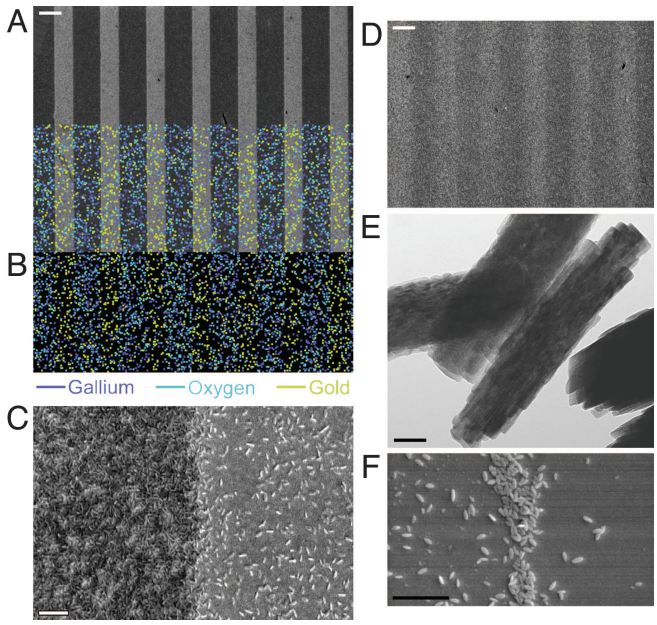

Fig. 3. Products of wafer-catalyzed and templated reaction. (*A*) Scanning electron microscopy images depicting products formed from the hydrolysis and condensation of the gallium nitrate precursor catalyzed by the bifunctional wafer containing the nucleophilic (hydroxyl) and hydrogen-bonding (imidazole) termini (NP-HB surface). (Scale bar: 10 μm.) A 10-fold greater particle number density is observed on the hydroxyl lines than on the imidazole lines. (*B*) Energy-dispersive spectrometry mapping of condensate on the NP-HB biomimetic catalyst revealing the product, localized on the hydroxyl lines, rich in gallium and oxygen. (*C*) Higher-magnification imaging reveals a dense network of layered particles condensed upon hydroxyl-printed lines. (Scale bar: 1 μm.) (*D*) Substitution of either essential surface functionality (nucleophile or hydrogen-bonding amine) with a nonactive methyl group renders the surface hydrolytically inactive. (Scale bar: 10 μm.) (*E*) Particles from hydroxyl-terminated SAMs from *C*. (Scale bar: 50 nm.) (*F*) Sample removed after a short reaction time demonstrates significantly more condensed product at the SAM interface, with a substantial decrease in particle number density away from the interface. (Scale bar: 1 μm.)

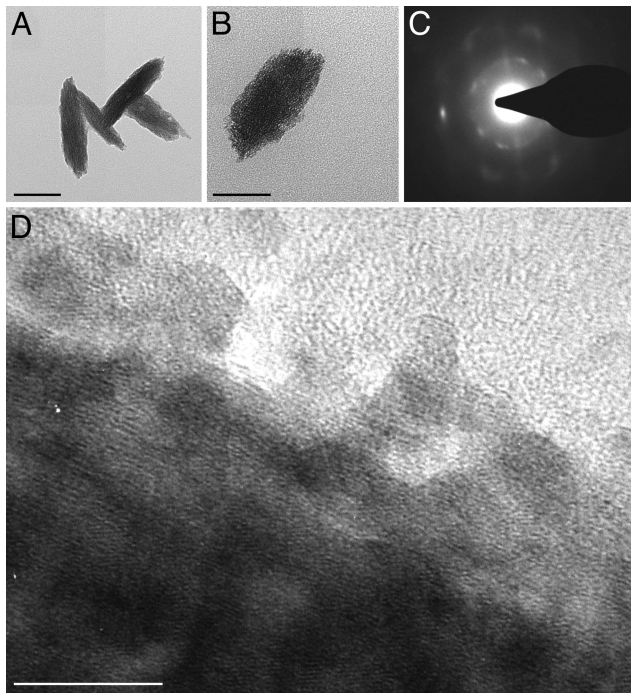

Fig. 4. TEM images showing γ-Ga_2O_3 particles formed on the hydroxyl-terminated SAMs (*A*) and GaOOH particles formed on the imidazole-terminated surface (*B*). (Scale bars: 100 nm.) (*C*) Selected-area electron diffraction pattern of *A* confirming the γ-Ga_2O_3 structure. (*D*) High-resolution TEM image of *A* demonstrating that the larger particle is made of smaller nanocrystals that are co-aligned in the core of the particle but not aligned at the periphery. (Scale bar: 10 nm.)

aggregates seem to follow an alignment at the core of the particle whereas those at the periphery tend to be misaligned.

Discussion

SAM Formation and Functionalization. Upon contact with the surface, the functionalized alkane thiols adsorb to the gold surface via the formation of strong gold–sulfur bonds (22). Additional van der Waals forces between the long alkane chains forces a self-assembly into a well packed two-dimensional crystal with the ω-functionality exposed at the film–air interface (22, 24). As expected, contact-angle measurements (Table 1) of the SAMs displaying the polar headgroups (e.g., OH and COOH) were lower than for those presenting the more hydrophobic groups, although somewhat higher (>5°) than seen in other studies (22). Possible reasons for this discrepancy could include contamination of the gold substrate by surface impurities before SAM deposition or incomplete packing of the alkane thiolate chains (24). Incomplete packing usually results from short hydrocarbon chain lengths [i.e., $(CH_2) < 8$] or insufficient time for absorption and chain rearrangement (22, 24).

Catalysis. The proximity of the imidazole headgroup to the hydroxyl moiety on the bifunctional surface (approximately <5 Å) optimizes the close approach of the imidazole's nitrogen to the hydroxyl's hydrogen atom such that hydrogen bonding may occur (Fig. 1*A*). This juxtaposition of functional groups is facilitated through dense packing of alkane thiolates on the (111) gold surface (24, 25).

Because the gallium nitrate hydrate precursor solution is acidic, it would be expected that hydrogen bonding with neighboring hydroxyls would be inhibited because of protonation of the nitrogen. However, low-field proton shifts observed in NMR studies of the catalytic site in α-chymotrypsin (a serine protease that is active at low pH) confirmed the presence of hydrogen bonding between the histidine and serine residues even at low pH (26, 27). Although the pK_a of the hydrogen-bonding moieties were not measured in this study, there are a number of effects that can broaden the titration curve, effectively lowering the pK_a of the imidazole by as much a 3 pH units. Thus, for example, unusually low pK_a values have been documented for histidine buried within the hydrophobic core of the *Bacillus circulans* xylanase (28) and for histidine residues in a similar environment in cyclophilin (29). It also has been shown that the electrostatic repulsion between adjacent and closely packed charged amine functionalities (as on our SAM surfaces) screens these groups from protonation and reduces their effective pK_a by as much as 3 pH units (30–32). This situation is similar to that found in the catalytic sites of many hydrolases. For example, in silicatein α, hydrogen bonding can occur between the hydroxyl group of serine 26 and the imidazole residue of histidine 165, because of their close proximity (estimated to be within 3 Å) in the active site, thereby increasing the nucleophilicity of the serine oxygen (6). Similarly, we suggest that the enhanced nucleophilicity of the hydroxyl side chains at the interface with the amine functionalities on the bifunctional wafer could facilitate an attack on the gallium atom in gallium nitrate hydrate to form a transitory Ga–O bond, initiating deprotonation and subsequent partial or complete hydrolysis of the soluble species (33, 34). This reaction is closely analogous to that believed to occur between silicatein and its substrates (including gallium nitrate hydrate) (10) in its active site (1, 2, 4, 6). Hydrolytic activity toward the gallium nitrate hydrate complex was reduced on the bifunctional wafers that lacked either nucleophile or

hydrogen-bonding moieties (when replaced with an nonactive methyl group) by an order of magnitude (≈1.20 ± 0.13 particles per μm^2 on the surfaces of nonactive mimics), confirming previous observations made with silicatein (6) and the biomimetic gold nanoparticle-supported SAMs (17). We suggest that even greater increases in this ratio could have been made by sequentially replacing the gallium nitrate hydrate solutions at shorter time intervals, thereby reducing the contribution from homogeneous nucleation in solution.

The gallium oxide precursor, gallium nitrate, $Ga(NO_3)_3{\cdot}6H_2O$ (GNO), is a highly soluble and stable metal oxide precursor. After dissociation of the metal salt by water, hydration of the GNO system is thermodynamically favored by the large enthalpy of hydration (approximately −1,100 kcal/mol) (35). Autohydrolysis in this complex by means of deprotonation is minimal as a result of the relatively large diameter of the 3+ gallium cation (0.60 Å; versus 0.45 Å for 3+ aluminum), which provides additional electron shielding for the nucleus. Thus, gallium hydrate does not form hydrolyzed complexes in the absence of external catalysis. The nature and stability of the GNO precursor can be predicted by using the partial charge model (34), which determines the partial charges on the cation and its surrounding ligands (e.g., hydroxyl groups, water molecules) after achieving equilibrium of their electronic chemical potentials. Based on this model, a stable, fully hydrated gallium complex is expected at low pH (≈3) and room temperature. Thus, for hydrolysis leading to formation of the metal oxide to occur, a nucleophilic attack is required to polarize the Ga–OH_2 bond, leading to deprotonation. We propose that the enhanced nucleophilicity resulting from the juxtaposition of NP and HB functionalities at the interface between these zones on the bifunctional SAM polarizes the GNO precursor, leading to the destabilization of a proton on one or more of the hydrated ligands. The resulting hydrolyzed species {e.g., $[Ga(OH)_2(OH_2)_4]^{+1}$} can then undergo condensation reactions with other soluble gallium (monomeric or polymeric) species such as gallium hydroxide; additionally, condensation of these hydrolyzed species may occur with hydroxyls presented on the SAM through olation or oxolation to form extended metal oxide structures. It also is possible that condensation reactions may have occurred in solution, leading to homogeneous precipitation followed by adsorption to the SAM surface; future experiments should help elucidate the relative contributions of these condensation mechanisms.

An additional experiment was performed to confirm the necessity of the hydrogen-bonding agent for enhancement of the nucleophilicity and resulting hydrolytic activity of the hydroxyl SAM. Exogenous histamine (0.05 mM, final concentration), a hydrogen-bonding imidazole, was mixed in solution with the gallium oxide precursor (pH ~ 3) in the presence of a hydroxyl-terminated SAM. Significant product formed on the hydroxyl-terminated wafer whereas no product was observed on samples either presenting a methyl-terminated surface with exogenous histamine or a hydroxyl-terminated wafer without histamine. Similar results were seen when using exogenous histamine to rescue the catalytic activity of a genetically engineered silicatein that had been made inactive by replacement of the active-site histidine with a non-catalytically active (methyl-terminated) alanine (M. Merget and D.E.M., unpublished work).

Although the presence of linear arrays of the nucleophilic hydroxyl and hydrogen-bonding imidazole SAMs do not offer the exact geometry of the enzymatic precursor-binding cleft and its integral catalytic active site, the juxtaposition of these two species at each linear interface allows for the same interaction between these two groups and the metal oxide molecular precursor. Confirmation of the catalytic activity of this juxtaposition interface was demonstrated by examination of a sample removed a short time after immersion in the reagent solution (Fig. 3*F*). Although this finding supports the presence of a catalytic site at the line interface, a measurable amount of product also was found away from this interface. We suggest that nucleation of gallium oxide nanocrystals on the hydroxyl SAM regions indicates that catalytically active surface groups present at the interface between the two classes of functionalized lines were directly responsible for hydrolysis, and that additional hydroxyl groups on the surface then served as sites for subsequent condensation of the hydrolyzed gallium species. As described above, nonfunctional or monofunctional SAMs (containing juxtaposition interfaces of the hydroxyl or imidazole lines with methyl-terminated lines) did not initiate hydrolysis or condensation of the GNO precursor, confirming the requirement for the combination of nucleophile and hydrogen-bonding functionalities. Hydroxyl-rich nucleation surfaces, tested alone as a control, initiated no precipitation.

Phase Identification and Mechanism of Growth (Nucleation and Condensation). It is intriguing that both GaOOH and γ-Ga_2O_3 phases were identified in the product. The presence of GaOOH is expected via the direct hydrolysis of a hydrated gallium complex. This product is routinely obtained after treatment with strong alkali, which initially yields gallium hydroxide and through a condensation reaction yields GaOOH. The formation of GaOOH, which has a lamellar structure (e.g., Fig. 4*B*), is the thermodynamically favored phase (36) at room temperature. However, additional dehydration of the oxohydroxide can also yield the oxide via the reaction

$$2\ GaOOH \rightarrow Ga_2O_3 + H_2O. \qquad [1]$$

Identification of this unique reaction product supports the notion that the NP-HB interface catalyzed the hydrolysis of the hydrated precursor to first yield an unstable gallium hydroxide [$Ga(OH)_3$] that was undetected in these experiments, and that through subsequent condensation reactions these produced GaOOH (as typically formed by base catalysis). The pathway of subsequent dehydration to form the oxide in these experiments is currently unknown. Although more thermodynamically stable species should form from direct hydrolysis at room temperature, kinetic barriers may limit their formation to yield more disordered, hydrated forms in the following sequence:

$$\text{amorphous-}Ga(OH)_3 \rightarrow GaOOH \rightarrow Ga_2O_3. \qquad [2]$$

Two potential pathways exist. One involves formation of the oxide through dehydration driven by condensation of oxohydroxide on the hydroxyl SAM surface (a low surface energy amenable to wetting by the oxohydroxide). A second potential pathway involves adsorption with subsequent dissolution and reprecipitation of the oxohydroxide, which has a significant solubility at low pH (33), to yield the oxide.

Immediately after deprotonation, the hydrolyzed species may diffuse to and condense with the hydroxyl moieties on the SAM, initiating nucleation of surface embryos that can continue to grow by accretion. However, the monodispersity of the particles we observed tends to negate this possibility. An alternative possibility is that the hydrolyzed gallium species condenses with other soluble hydrolyzed complexes, forming homogeneously nucleated embryos that electrostatically adsorb to the hydroxyl surface. Such embryos and nuclei would most likely be GaOOH although there is no direct evidence for this. A third alternative pathway may involve the surface hydroxyls on the SAMs participating as templates similar to those on the silicatein surface (10), with a low surface energy reducing the activation energy to nucleation (37) of the newly formed subcritical embryos of hydrolyzed $Ga(OH_2)_6$. We suggest that these hydroxyl groups on the SAM surfaces may hydrogen bond with the hydrolyzed species, with ripening or dissolution–reprecipitation of the species [known to occur at low pH (33)] and subsequent dehydration to γ-Ga_2O_3. The significantly larger GaOOH particle size on the imidazole lines (relative to particles on the OH-terminated SAMs) can be explained by the difference in

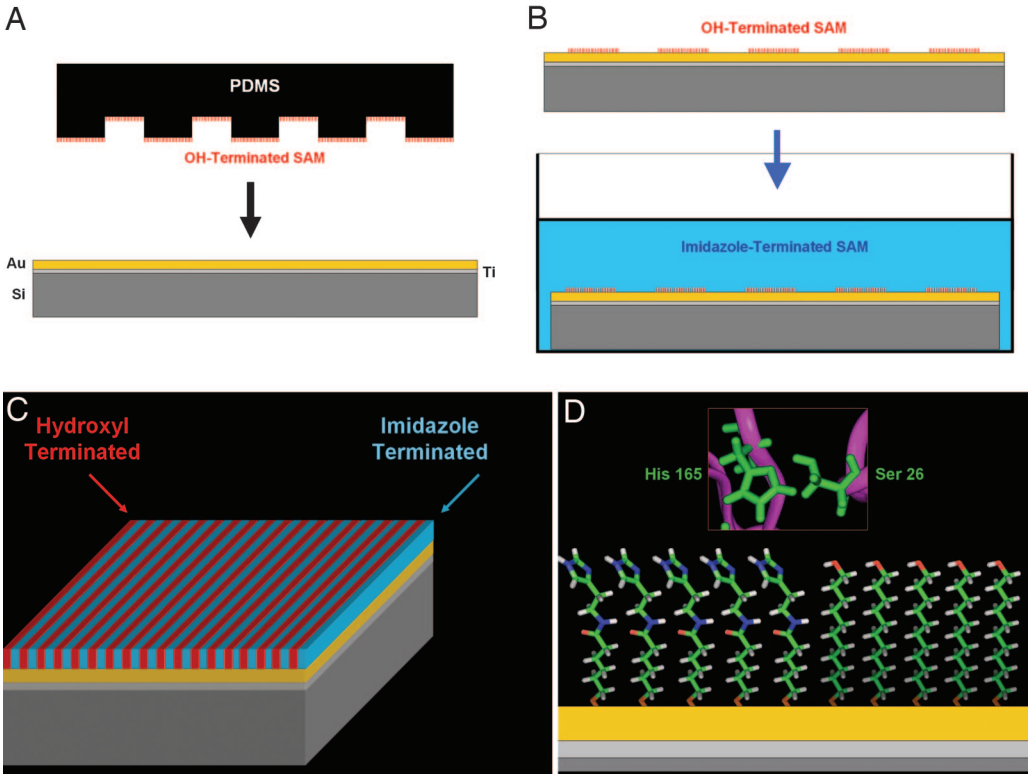

Fig. 5. Schematic depicting the formation of a bifunctional SAM. (*A*) A poly(dimethylsiloxane) (PDMS) stamp inked with an alkane thiolate (e.g., OH-terminated) is brought into contact with a gold surface, facilitating transfer of the thiol to the gold through adsorption with sulfur (23). (*B*) After the initial printing of the first alkane thiol, the wafer is then immersed in a different alkane thiol (e.g., imidazole-terminated) solution to form the second monolayer resulting in a bifunctionalized SAM surface (*C*) that presents the essential functionalities necessary for hydrolysis (*D*), similar to those found in silicatein.

surface energies. In addition to lacking the necessary condensation sites for the hydrolyzed species, the less hydrophilic imidazole surface (Table 1) has a higher surface energy than the hydroxyl SAM and thus presents a larger barrier to nucleation.

Further insight into the condensation mechanism is obtained from high-resolution transmission electron micrographs (Fig. 4*D*) of particles formed on the SAM surface. Evidence shows that these particles consist of oriented aggregates of smaller (≈3 nm) nanocrystalline particles, suggesting that hydrolysis of the gallium nitrate hydrate leads to the formation of nanocrystals that through adsorption–dissolution–reprecipitation processes form larger single crystal-like particles.

Observation of dense lines of γ-Ga_2O_3 that had detached from the OH-terminated SAM surface revealed the presence of pores spaced ≈200 nm apart. Aizenberg's studies of the dehydration of amorphous calcium carbonate showed that pores of similar dimension can serve as pathways for the removal of water, driving the dehydration to form calcite from amorphous calcium carbonate (38). A similar mechanism may be operative in the system we have described.

We have demonstrated the development of a biomimetic analog of a biosilica- and semiconductor-forming enzyme isolated from a marine sponge. Micropatterned juxtaposition of nucleophilic (hydroxyl) and hydrogen-bonding (imidazole) functionalities in the proper geometry enhanced the activity of the nucleophilic moieties that act as a catalyst for the hydrolysis of a gallium oxide precursor to form gallium oxide and GaOOH. Replacement of either nucleophile or hydrogen-bonding functionality with a nonactive methyl-terminated SAM significantly reduced the catalytic activity. Samples removed after short reaction times showed product forming near the interface of the printed lines confirming the catalyst location. The presence of the oxohydroxide and oxide on the SAM surfaces indicated a kinetically limited transitory dehydration similar to that seen with other hydrated cation systems that proceed incrementally through successive stages of dehydration, with progressively lower activation energy barriers, to finally reach their thermodynamically stable states.

Although this work has potentially broad application for the surface-catalyzed low-temperature synthesis of novel materials with catalytic, electronic, and optical properties, further understanding of mechanisms involved in hydrolysis of aqueous mineral systems is needed.

Materials and Methods

Gold Wafer Preparation. Gold-coated silicon wafers were prepared at room temperature by evaporating a thin adhesion layer (≈2 nm) of titanium onto (100) silicon wafers (University Wafer, Boston) followed by a top layer of gold (≈48 nm). Freshly coated wafers were stored in a desiccator until use.

Bifunctionalization with SAMs. Bifunctional SAM wafers were prepared by inking a relief-structured (5-μm plateaus × 10-μm channels) poly(dimethylsiloxane) stamp (39) with a 5 mM ethanolic solution of ω-functionalized (ω = carboxylic acid, methyl, or amino) undecane thiol [ω-$(CH_2)_{10}$-SH; Sigma-Aldrich and Dojindo Molecular Technologies (Gaithersburg, MD)]. After depositing a drop of 5 mM alkane thiol onto the surface, stamps were spin-coated (Chemat Technology, Northridge, CA) at 3,000 rpm to remove excess solvent. Inked stamps were then placed in contact (Fig. 5*A*) with the gold substrates for 20 min to allow transfer of alkane thiol to the gold surface to facilitate a reaction between the sulfhydryl group (−SH) and the gold (22). Stamps were carefully removed, and the freshly monofunctionalized wafer was subsequently rinsed

with ethanol. After monofunctionalization, wafers were immersed in a different ω-terminated alkane thiol solution for 1 h (Fig. 5*B*). Bare regions of gold that were not printed with the primary thiol were subsequently susceptible to reaction with the second alkane thiol to subsequently produce a densely packed, bifunctional surface (Fig. 5*C*) in which the interface between the amine and hydroxyl functionalities mimics the catalytic site in silicatein (Fig. 5*D*).

Synthesis of Imidazole-Terminated SAMs. A carboxylic acid-terminated SAM was initially printed on the gold layer followed by derivatization to an imidazole moiety through a coupling reaction that converts the carboxylic acid group into the imidazole via an intermediate formed with 1-ethyl-3-(3-dimethylaminopropyl)-carbodiimide (Sigma-Aldrich) and *N*-hydroxysuccinimide (Sigma-Aldrich) that is susceptible to attack by amines (40). In this reaction, the carboxylic acid-terminated SAM was immersed in a 5 mM ethanolic solution of 1-ethyl-3-(3-dimethylaminopropyl)-carbodiimide and *N*-hydroxysuccinimide for 1 h. Reactive SAM functionalized wafers were then rinsed with ethanol, immediately immersed in a 5 mM ethanolic solution of histamine (Sigma-Aldrich) overnight, and rinsed with ethanol. Formation of the second ω-terminated alkane thiol followed the immersion method described in the previous section.

Monofunctionalization of Wafers and Contact-Angle Measurements. To confirm ω-terminated SAM deposition and uniformity, monofunctionalized wafers of ω-terminated SAMs were prepared by immersing gold wafers in 5 mM ethanolic solutions of various alkane thiols for 1 h. After functionalization, wafers were removed from the alkane thiol solution, rinsed with ethanol, and dried. Contact-angle measurements (advanced and receding) were performed on each derivatized surface (23). For these measurements, microliter-sized droplets of Milli-Q-purified (Millipore) water were dispensed through a syringe onto the SAM surfaces, and five measurements were taken per sample.

Reaction of Bifunctional SAMs with Gallium Oxide Precursor. Bifunctional wafers [hydroxyl–imidazole, hydroxyl–methyl, methyl–imidazole, and hydroxyl–gold (no SAM)] were placed upside down in Teflon holders and subsequently immersed in 50 mM aqueous solutions of gallium nitrate hydrate (pH $\sim$ 3) for 72 h. Wafers were then removed from the precursor solution, rinsed thoroughly with deionized water, and dried under a stream of air.

Scanning Electron Microscopy and Energy-Dispersive Spectroscopy. Surface features of reaction products were imaged by using a cold cathode field-emission scanning electron microscope (JEOL JSM 6300F) equipped with an energy-dispersive spectrometer. Specimens were mounted on conductive carbon adhesive tabs (Ted Pella) and examined (at 5 or 10 kV) either uncoated (for energy-dispersive spectrometry analysis) or after gold/palladium sputter coating (for imaging). Energy-dispersive spectrometry (Oxford Instruments, Palo Alto, CA) was performed in conjunction with scanning electron microscopy to qualitatively determine the chemical composition of specimens.

TEM. The reaction products were scraped off the wafer surfaces into water and ultrasonicated to form a suspension. TEM specimens were prepared by pipetting a small amount ($\approx$20 μl) of the particle suspension onto holey carbon copper grids (Ted Pella). The grids were then dried at room temperature and imaged with a transmission electron microscope (FEI T20) to observe particle morphologies and obtain structural information by means of selected-area electron diffraction. Lattice imaging was performed with a high-resolution transmission electron microscope (JEOL 2010). Both of the transmission electron microscopes were operated at 200 kV. Samples were imaged at magnifications from $\times$20,000 to $\times$200,000 in the conventional transmission electron microscope and from $\times$500,000 to $\times$800,000 in the high-resolution transmission electron microscope. Selected-area electron diffraction patterns were obtained at camera distances of 55, 83, and 100 cm. A standard evaporated aluminum film (lattice constant = 0.4041 nm) was used as a standard for calibration of the camera.

We thank Ombretta Masala for expert assistance with high-resolution TEM analysis. This work was supported by U.S. Department of Energy Grant DE-FG03-02ER46006, Institute for Collaborative Biotechnologies Grant DAAD19-03-D-0004 from the U.S. Army Research Office, National Aeronautics and Space Administration Grants NAG1-01-003 and URETI-00000532, the National Oceanic and Atmospheric Administration National Sea Grant College Program, U.S. Department of Commerce Grant NA36RG0537 (Project R/MP-92) through the California Sea Grant College System, and the Materials Research Science and Engineering Centers Program of the National Science Foundation under Award DMR-96-32716 to the University of California, Santa Barbara, Materials Research Laboratory. Y.A. was supported by the Japan Society for the Promotion of Science.

1. Roco, M. C. (2003) *Curr. Opin. Biotechnol.* **14,** 337–346.
2. Dodson, G. & Wlodawer, A. (1998) *Trends Biochem. Sci.* **23,** 347–352.
3. Shimizu, K., Cha, J., Stucky, G. D. & Morse, D. E. (1998) *Proc. Natl. Acad. Sci. USA* **95,** 6234–6238.
4. Cha, J., Shimizu, K., Zhou, Y., Christiansen, S. C., Chmelka, B. F., Stucky, G. D. & Morse, D. E. (1999) *Proc. Natl. Acad. Sci. USA* **96,** 361–365.
5. Murr, M. M. & Morse, D. E. (2005) *Proc. Natl. Acad. Sci. USA* **102,** 11657–11662.
6. Zhou, Y., Shimizu, K., Cha, J. N., Stucky, G. D. & Morse, D. E. (1999) *Angew. Chem. Int. Ed.* **38,** 779–782.
7. Morse, D. E. (1999) *Trends Biotechnol.* **17,** 230–232.
8. Morse, D. E. (2001) in *The Chemistry of Organic Silicon Compounds*, eds. Rappoport, Z. & Apeloig, Y. (Wiley, New York), Vol. 3, pp. 805–819.
9. Sumerel, J. L., Yang, W., Kisailus, D., Weaver, J. C. & Morse, D. E. (2003) *Chem. Mater.* **15,** 4804–4809.
10. Kisailus, D., Choi, J. H., Weaver, J. C., Yang, W. & Morse, D. E. (2005) *Adv. Mater.* **17,** 314–318.
11. Cha, J., Stucky, G. D., Morse, D. E. & Deming, T. J. (2000) *Nature* **403,** 289–292.
12. Roth, K. M., Zhou, Y., Yang, W. & Morse, D. E. (2005) *J. Am. Chem. Soc.*, in press.
13. Naik, R. R., Brott, L. L., Clarson, S. J. & Stone, M. O. (2002) *J. Nanosci. Nanotechnol.* **2,** 95–100.
14. Kröger, N., Bergsdorf, C. & Sumper, M. (1994) *EMBO J.* **13,** 4676–4680.
15. Kröger, N., Lehmann, G., Rachel, R. & Sumper, M. (1997) *J. Biochem.* **250,** 99–103.
16. Kröger, N., Deutzmann, R. & Sumper, M. (1999) *Science* **286,** 1129–1132.
17. Kisailus, D., Najarian, M., Weaver, J. C. & Morse, D. E. (2005) *Adv. Mater.* **17,** 1234–1238.
18. Constantine, C. A., Mello, S. V., Dupont, A., Cao, X., Santos, D., Oliviera, O. N., Strixino, F. T., Pereira, E. C., Cheng, T. C., DeFrank, J. J. & Leblanc, R. M. (2003) *J. Am. Chem. Soc.* **125,** 1805–1809.
19. Jaffrezic-Renault, N. (2001) *Sensors* **1,** 60–74.
20. Kharitonov, A. B., Zayats, M., Lichtenstein, A., Katz, E. & Willner, I. (2000) *Sensors Actuators B* **70,** 222–231.
21. Letant, S. E., Hart, B. R., Kane, S. R., Hadi, M. Z., Shields, S. J. & Reynolds, J. G. (2004) *Adv. Mater.* **16,** 689–693.
22. Bain, C. D., Troughton, E. B., Tao, Y. T., Evall, J., Whitesides, G. M. & Nuzzo, R. G. (1989) *J. Am. Chem. Soc.* **111,** 321–335.
23. Wasserman, S. R., Tao, Y. T. & Whitesides, G. M. (1989) *Langmuir* **5,** 1074–1087.
24. Ulman, A. (1996) *Chem. Rev.* **96,** 1533–1554.
25. Schreiber, F. (2000) *Prog. Surf. Sci.* **65,** 151–158.
26. Robillard, G. & Shulman, R. G. (1972) *J. Mol. Biol.* **72,** 507–513.
27. Molina, P. A. & Jensen, J. H. (2003) *J. Phys. Chem. B* **107,** 6226–6231.
28. Plesniak, L. A., Connelly, G. P., Wakarchuk, W. W. & McIntosh, L. P. (1996) *Protein Sci.* **5,** 2319–2324.
29. Yu, L. & Fesik, S. W. (1994) *Biochem. Biophys. Acta* **1209,** 24–29.
30. Palmer, B. N. & Powell, H. K. J. (1974) *J. Chem. Soc. Dalton Trans.* **19,** 2089–2095.
31. Guo, D. & Lu, Z. (2003) *J. Gen. Physiol.* **122,** 485–492.
32. Matulis, D. & Bloomfield, V. A. (2001) *Biophys. Chem.* **93,** 37–44.
33. Baes, C. F. & Mesmer, R. E. (1976) *The Hydrolysis of Cations* (Wiley, New York).
34. Henry, M., Jolivet, J. P. & Livage, J. (1992) *Chem. Spectrosc. Appl. Sol-Gel Glasses* **77,** 153–206.
35. Latimer, W. M., Pitzer, K. S. & Slansky, C. M. (1939) *J. Chem. Phys.* **7,** 108–111.
36. Roy, R., Hill, V. G. & Osborn, E. F. (1952) *J. Am. Chem. Soc.* **74,** 719–722.
37. Navrotsky, A. (2004) *Proc. Natl. Acad. Sci. USA* **101,** 12096–12101.
38. Aizenberg, J., Muller, D. A., Grazul, J. L. & Hamann, D. R. (2003) *Science* **299,** 1205–1208.
39. Xia, Y. & Whitesides, G. M. (1998) *Annu. Rev. Mater. Sci.* **28,** 153–162.
40. Staros, J. V., Wright, R. W. & Swingle, D. M. (1986) *Anal. Biochem.* **156,** 220–222.